Electron Beam Driven Plasma Wakefield of Photons

R. Sandberg^{1, a)} and A. G. R. Thomas^{1, b)}
Gérard Mourou Center for Ultrafast Optical Sciences, University of Michigan, Ann Arbor, MI 48109,
USA

(Dated: 23 October 2023)

The paper [R.T. Sandberg and A.G.R. Thomas, Phys. Rev. Lett. 130, 10.1103/PhysRevLett.130.085001 (2023)] proposed a scheme to generate ultrashort, high energy pulses of XUV photons though dephasingless photon acceleration in a beam driven plasma wakefield. An ultrashort laser pulse is placed in the plasma wake behind a relativistic electron bunch so that it experiences a density gradient and therefore shifts up in frequency. Using a tapered density profile provides phase-matching between driver and witness pulses. In this paper, we study via particle-in-cell simulation the limits, practical realization and 3D considerations for beam driven photon acceleration using the tapered plasma density profile. We study increased efficiency by use of a chirped drive pulse, establishing the necessity of the density profile shape we derived as opposed to a simple linear ramp, but also demonstrating that a piecewise representation of the profile—as could be achieved experimentally by a series of gas cells—is adequate for achieving phase matching. Scalings to even higher frequency shifts are given.

I. INTRODUCTION

The many applications of bright, coherent XUV light have motivated substantial interest in source development, such as the construction of XUV wavelength Free Electron Lasers such as FLASH⁴⁴ as well as nonlinear frequency mixing⁴⁵, high harmonic generation⁴⁶, relativistic flying mirrors^{47–49}, and XUV lasing⁵⁰, to name a few. Another method for generating short wavelengths is the scheme of 'photon acceleration's¹. In 'photon acceleration', a laser pulse that experiences a co-moving plasma density gradient will be upshifted in frequency. From eikonal solutions to the wave equation, well known ray-tracing solutions can be used for the temporal variation in the light^{52,53}, which for a plane wave propagating in the z direction with linear plasma dispersion ($\omega^2 = k^2c^2 + \omega_p^2$, where $\omega_p^2 = e^2n/m_e\varepsilon_0$ for a plasma of number density n) results in a frequency shift according to

$$\frac{d\omega}{dz} \simeq -\frac{1}{2kc^2} \frac{\partial(\omega_p^2/\gamma)}{\partial z} \ . \tag{1}$$

Photon acceleration can arise as a result of plasma wakefields⁵¹, ionization fronts^{54,55} and even using metamaterials⁵⁶. Photon acceleration was measured in ionization front⁵⁷ and laser wakefield acceleration experiments^{58,59}. Recent results include cascaded sequences of localized ionizations⁶⁰, resulting in large frequency shifts and the use of plasma wakes to downshift radiation to very long wavelengths⁶¹. Limits to photon acceleration in plasma wakefields in the linear⁶² and nonlinear regimes^{63,64} were previously studied, identifying dephasing of the photon beam with respect to the accelerating refractive index gradient placing a ceiling on the frequency shift. Dephasing occurs when the difference

between the phase velocity of the wake and the high-frequency photon pulse results in it slipping out of the accelerating refractive index gradient. A recent scheme for overcoming this restriction using an ionization front is dephasingless frequency shift using a 'flying focus,' a combination of a chirped laser pulse and an achromatic lens for spatiotemporal shaping of a laser pulse 65 . The flying focus was also used to mitigate the analogous process of electron beam dephasing in a plasma wakefield 66 , in addition to related spatiotemporally structured focusing schemes 67,68 .

Another method for mitigating dephasing, in the context of electron acceleration is the use of tapered plasma density ramps^{69–72}. By having a non-uniform density, the plasma wavelength varies along the propagation length, which allows for locking the accelerating phase with the particle beam. Tapered density ramps were previously suggested as a way of increasing the frequency shifts in photon acceleration^{51,62}.

For positive frequency shift, the laser pulse must be at a phase in the wake where the density is gradient is negative with respect to z. However, the laser centroid moves at the group velocity of the laser pulse and so as the laser pulse shifts in frequency, its group velocity increases and the pulse will change position in the wake. To mitigate dephasing of the photon pulse, we use a tapered density profile (similar to that proposed for mitigating dephasing in electron acceleration $^{70,72-74}$) to continuously increase the plasma wavelength and keep the laser pulse experiencing a positive plasma density gradient. We also use an electron beam driver, which both simplifies the phase matching condition and addresses issues with red shifting of the drive pulse in the case of a laser driver.

For phase matching, we must try to keep the witness pulse at the phase where the density perturbation in the wake $\delta n(\zeta;z) \equiv n_w(\zeta;z) - n(z) = 0$ within the region of negative density gradient, hereby labelled as ζ_{δ} , as the location of the reference density gradient we are trying to track. To keep the pulse experiencing the greatest possible frequency shift, we require $\zeta_{\text{centroid}} = \zeta_{\delta}$ for all

^{a)}Electronic mail: ryansand@umich.edu.

b) Electronic mail: agrt@umich.edu.

times, where $\zeta_{\rm centroid}$ denotes the center of the witness laser pulse. However, this is complicated by the fact that as the laser pulse shifts in frequency, its group velocity varies, leading to a system of coupled differential equations. Assuming that the laser pulse moves at the linear group velocity and the plasma is underdense, $\omega_p^2/\omega^2 \ll 1$, we previously obtained⁷⁵ an equation relating the z profile of the plasma number density to the variation in the wake position of the zero density perturbation ζ_δ with plasma density,

$$\frac{dn}{dz} \simeq \frac{1}{2c} \frac{\omega_p^2}{\omega^2} \left[\frac{d\zeta_\delta}{dn} \right]^{-1} . \tag{2}$$

The phase matching condition in equation 2 and the frequency shift relation in equation 1 together are a coupled pair of differential equations to be solved using an extension of 1D beam driven wakefield solutions⁷⁶ to obtain the plasma density profile that will give phase matched photon acceleration. Full details of the numerical solution and its derivation for the density profiles are being published elsewhere⁷⁷.

In this paper, we study via particle-in-cell simulation the limits, practical realization and 3D considerations for beam driven photon acceleration using the tapered plasma density profile demonstrated in Ref. ⁷⁵. The simulations show that it is possible to generate ultrashort pulses of XUV radiation with relativistic intensity, that is the normalized vector potential $a_0 = eE_0/m_ec\omega_0 \sim 1$, where E_0 is the peak field of the witness pulse. In the simulations, we use the density profile determined by solving equations (1) and (2) in a series of simulations to demonstrate the behavior of dephasingless plasma wakefield photon acceleration (dePWPA) for deviations from ideal conditions.

- We first demonstrate the importance of the phase matched density profile by comparing a simulation of a uniform plasma density profile and various linear plasma densities with the phase matched profile. The laser pulse rapidly dephases from the upshifting region of the wake in every non-dePWPA case.
- Next we use realistic beam parameters to demonstrate 10× frequency shift. Later, this simulation will then be repeated in 3D; comparison indicates the effective 1D nature of the scheme even in 3D geometry.
- We perform a 1D simulation with a long drive beam to demonstrate a beam profile not obtainable in the ultrashort limit. This simulation demonstrates $30 \times$ frequency shift and $6 \times$ energy gain.
- We repeat the previous simulation with a piecewise constant approximation to the density profile and still realize 30× frequency shift. A piecewise constant profile could be realized in practice with a series of gas cells.

- We perform a quasi-3D simulation demonstrating $10 \times$ frequency shift and $5 \times$ energy gain using the 1D phase matching profile, demonstrating the utility of the analytic profile in practice.
- Finally, we demonstrate 10× frequency shift and 5× energy gain in quasi-3D using a piecewise approximation to the phase matched profile. This demonstrates the robustness of the phase matched profile to non-ideal conditions.

We end by summarizing the results of the simulations and looking ahead to future research into photon acceleration.

For the simulations, we use the 1D version of the particle-in-cell (PIC) code OSIRIS^{78,79} and the quasi-3D code FBPIC⁸⁰. In the discussion of the 1D examples we introduce the normalizations when describing physical quantities. In the discussion of the 3D examples, physical quantities are detailed in SI units. The efficiency of energy transfer from the drive beam to the witness laser is an important metric that we study in both 1D and 3D situations. To measure the efficiency of the dePWPA scheme, we define the average energy transfer efficiency as

$$\eta = \frac{\Delta U_{laser}}{-\Delta U_{beam}} = \frac{U_{laser} - U_{laser,initial}}{U_{beam,initial} - U_{beam}},$$
 (3)

with energy changes $\Delta U_{laser/beam}$ measured between the initial and final times. In the 1D case, to calculate the energy transfer a characteristic area must be assumed in the non-simulated dimensions, which divides out of this expression. In all cases, for a "flat-top" particle beam driver of number density n_d and length L_d , the beam driver strength is parameterized by the normalized areal density of the beam $A=(n_d/n_0)k_{p0}L_d$, where n_0 is a reference plasma density and $k_{p0}=\omega_{p0}/c$.

II. 1D SIMULATION RESULTS

We start by simulating the dePWFA scheme under different drive beam, plasma profile and witness laser conditions in one dimension. To demonstrate the scaling of the solutions, for all the 1D simulations we express the equations in normalized units, with all plasma densities $n \to n/n_0$, such that $\omega_p \to \omega_p/\omega_{p0}$, $\omega \to \omega/\omega_{p0}$, $p \to p/m_e c$, etc., where $\omega_{p0}^2 = e^2 n_0/m_e \varepsilon_0$, $E \to eE/mc\omega_{p0}$, etc.

A. 1D simulations with and without the dePWPA density profile

Here, we use 1D simulations to compare the position of the laser in the case of the tapered plasma density profile with several other possible density profiles, including a piecewise constant approximation to the tapered profile, a uniform plasma density profile, and several linearly varying plasma densities.

In the simulations in this section, the drive beam has density $n_d/n_0=0.4$ and length $k_{p0}L_d=1.0$ for A=0.4. Initially the witness laser has $\omega_L/\omega_{p0}=10$. The witness laser has a normalized strength parameter $a_0=0.5$, with a pulse duration $\omega_{p0}\tau=0.885$, corresponding to an intensity full-width at half-max (FWHM) of 3 fs when $\lambda_0=800$ nm. We start with 618 cells per laser wavelength λ and in the tailored density case end with 61.8 cells per λ for the upshifted laser. We use a CFL condition of $\omega_{p0}\Delta t=0.9995k_{p0}\Delta x$ and 4 particles per cell.

We see in figure 1 the position of the laser centroid in the wake as a function of propagation distance for various plasma density profiles. The top panel shows the laser centroid and wake in the case of uniform plasma density, the middle panel shows the laser centroid and wake in the dePWPA plasma density profile, and the bottom panel shows the laser centroid and wake in a piecewise constant approximation to the dePWPA profile. In the uniform density case, the laser centroid clearly slips past the density peak and out of the frequency-shifting region, back into the density gradient of the next density peak, past that and on through the wake. No sustained frequency shift is attained. On the other hand, in the tapered density profile and its piecewise constant approximation the laser centroid maintains its position in front of the first density peak in the wake, where the density gradient is increasing with respect to ζ and the frequency shifts up continuously, as shown in Ref. 75.

In the bottom panel, the piecewise constant approximation is also able to maintain the centroid position on the density gradient on average. Through each constant section the centroid slips back, starting on a shallower part of the gradient than ζ_{δ} and ending up on a steeper gradient. The average gradient is very close to the gradient at ζ_{δ} and so the frequency shift and phase matching is near identical to the analytic solution density function shown in the middle panel. This result shows that the tapered density profile can be approximated by a piecewise constant representation with negligible degradation of performance. This is important because a piecewise constant profile could be achieved in practice by a series of gas cells or gas jets with different gas densities, whereas the analytic curve would be difficult to generate experimentally.

In previous papers, e.g.⁵¹, it has been suggested that a linear ramp would be able to mitigate dephasing. We have also simulated linear ramps of various gradients to try to mitigate dephasing. In Fig. 2, left hand panel, the position of the laser centroid in the wake is shown for various linear profiles. The linear down-ramped density profiles are chosen to have gradients from near the steepest in the dePWPA profile to the shallowest, as shown in the right hand panel of the figure (and also compared with the dePWPA profile). In addition to a limitation of the linear gradient that it eventually reaches zero and truncates the acceleration in any case, additionally the linear profile causes rapid dephasing for all linear gradients in-

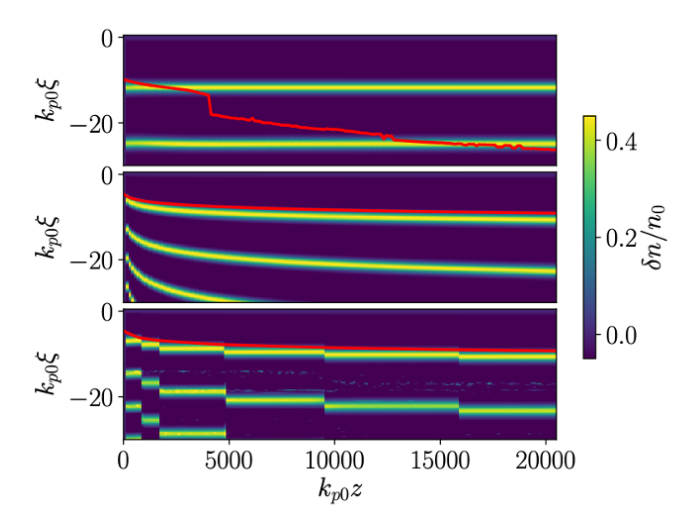


FIG. 1: Laser centroid in wake over propagation distance, comparing the effect of the (piecewise approximation to the) tapered density profile on the laser centroid. The centroid dephases rapidly from the wake in the uniform density case shown in the top panel, whereas the phase of the laser in the wake is maintained in the tapered density case shown in the bottom panel. To illustrate the wake we plot $\delta n = n_w(\xi; z) - n(z)$. Note that in these images the wake coordinate is

 $\xi = z - ct \text{ not } \zeta$, but for $v_p \to c$, $\xi \simeq -c\zeta$.

vestigated; indeed any linear gradient is arguably worse than a straightforward uniform gradient. This can be clearly seen from the left hand panel showing the wake-fields resulting from the linear ramp. The reason is that the curvature of the wakefield phase fronts is clearly the wrong way compared to the curvature of the centroid position for the analytically phase-matched profile, as in figure 1 middle panel. It is therefore clear that the de-PWPA solution, or at least an approximation to it, is required to achieve phase matching and hence large frequency shifts in PWPA.

B. 1D dePWPA simulation with a chirped driver for comparison with quasi-3D simulation

In this section we perform a 1D simulation using the dePWPA density profile and drive beam parameters for comparison with a later quasi-3D simulation, in particular using a chirped drive beam to increase energy transfer efficiency. This is because a finite length beam will generate a wakefield with a gradient such that the back of the drive bunch is decelerated faster than the front. By adding a chirp, the beam energy loss can be tuned so that the whole beam depletes at once, which increases the energy transfer efficiency from driver to witness. Initially the laser has $\omega_L/\omega_{p0}=10$. The drive beam has density $n_d/n_0=0.2$ and length $k_{p0}L_d=1.9$. These parameters correspond to A=0.38, which is the A used in

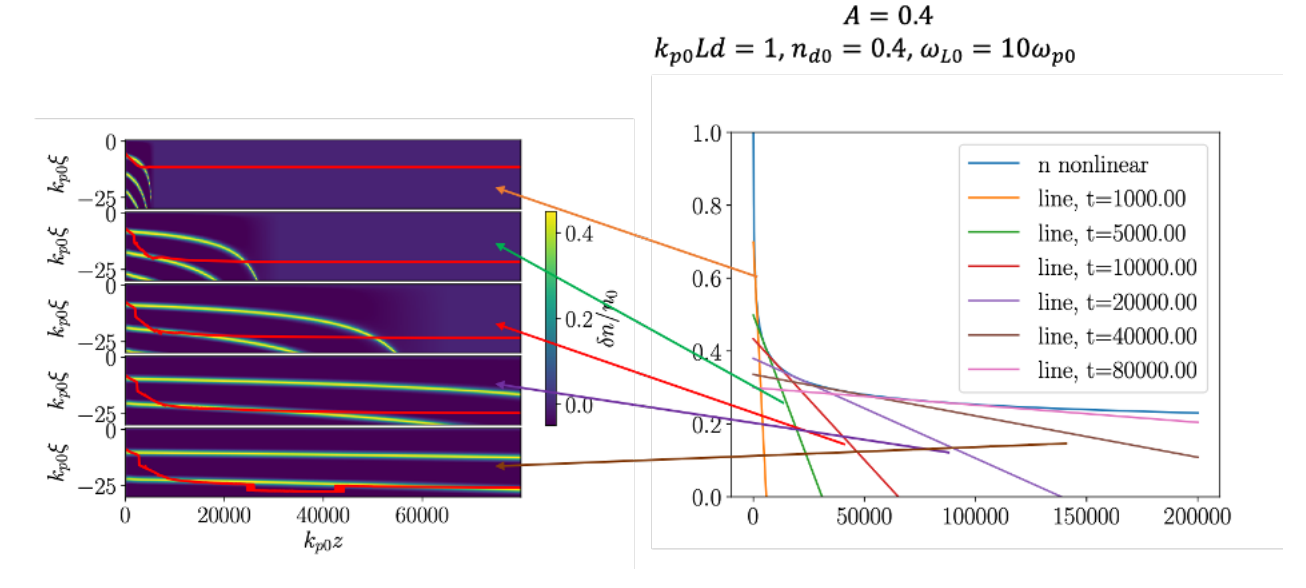


FIG. 2: Laser centroid in wake over propagation distance, comparing the effect of various linear plasma density profiles on the laser centroid. On the right is shown how the various linear profiles compare with the dePWPA profile. The centroid dephases rapidly from the wake regardless of the linear profile used. To illustrate the wake we plot $\delta n = n_w(\xi; z) - n(z)$. Note that in these images the wake coordinate is $\xi = z - ct$ not ζ , but for $v_p \to c$, $\xi \simeq -c\zeta$.

the later quasi-3D simulation. The laser has an $a_0=2.4$, with a pulse duration $\omega_{p0}\tau=0.885$, corresponding to an intensity full-width at half-max (FWHM) of 3 fs when $\lambda_0=800$ nm. We start with 618 cells per λ and in the tailored density case end with 61.8 cells per λ . We use a CFL condition of $\omega_{p0}\Delta t=0.9995k_{p0}\Delta x$ and 4 particles per cell.

We can see in figure 3 that the mean laser wavenumber matches the predicted wavenumber and increases by a factor of more than 10. The drive beam is linearly chirped in energy so that each section of the beam is depleted at roughly the same time. The chirp has the trapezoidal form $\gamma(\omega_{p0}\zeta) = 4000 + 32000(\omega_{p0}\zeta/1.9)$. The form of the chirp is chosen so that most of the drive beam energy is extracted, and 7.2% of the extracted energy is transferred to the witness laser pulse. The frequency shift and energy change stop around 120,000 $k_{p0}z$, at which point the drive beam is depleted of energy.

C. 1D long drive beam

In this section we demonstrate the ability of the model to generate frequency shift for finite length drive beams. We can see shifts of $30\times$ in frequency, $6\times$ in energy, $25\times$ in intensity, and $13\times$ in compression. The frequency gain stops once the driver is depleted of energy, indicating that the gain is limited only by the ability of the driver to maintain the wake.

The drive beam has density $n_d/n_0 = 0.3$ and length $k_{p0}L_d = 12.56$. The beam has an up-chirp in energy similar to the previous section of the form $\gamma(\omega_{p0}\zeta) =$

 $4000 + 32000(\omega_{p0}\zeta/12.56)$. The chirp helps prevents partial beam depletion but is not optimal; we anticipate that a triangular chirp would be more beneficial. Initially the laser has $\omega_L = 10$. The laser has an a_0 of 4.0, with an intensity pulse duration $\omega_{p0}\tau = 0.85$. We use 30000 cells for 618 cells per λ_{L0} and about 21 cells per λ_{Lf} , a CFL condition of $\Delta t = 0.9995\Delta x$, and 4 particles per cell.

Figure 4 shows that the mean laser wavenumber matches or exceeds the predicted wavenumber and increases by a factor of more than 30. About 5% of the energy lost by the drive beam is transferred to the witness laser pulse. The rate of change in energy transfer has a discontinuity around $60,000k_{p0}z$. This is the drive beam depletion length; at this point a portion of the beam has lost enough energy to move at sub-relativistic velocities and gets caught by the electron-accelerating fields. This loads the wake, so the laser pulse behind no longer sees an increasing density gradient and doesn't experience any more frequency shift.

The reported values of this 1D dimensionless simulation can be understood in physical units if we impose some initial scales. Assuming the initial laser wavelength is 800 nm and the drive beam has an initial root-mean-square radial extent $\sigma_r=16~\mu\mathrm{m}$, then the system propagates about 10 cm and the shifts are 30× in frequency, from an initial wavelength $\lambda=800$ nm to 27 nm, 6× in energy, from U=50 mJ to 900 nm, 25× in intensity, and $13\times$ in compression, from an initial full-width half-maximum in intensity pulse duration of $c\tau=900$ nm to 69 nm.

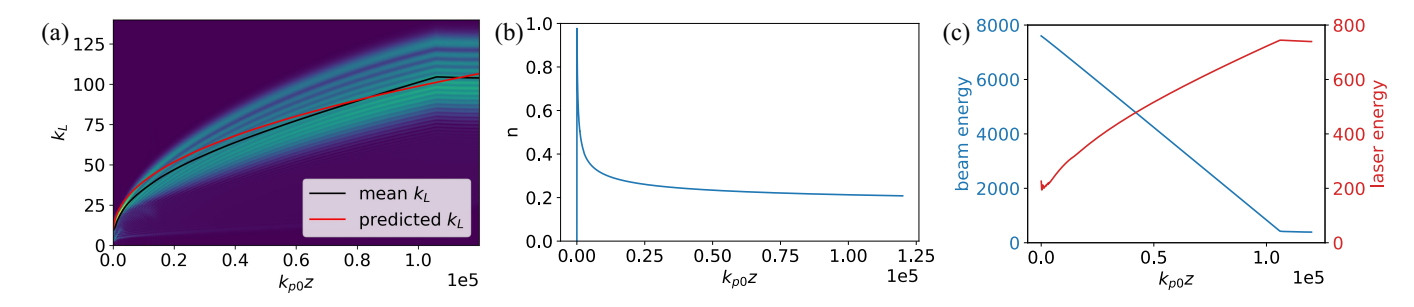


FIG. 3: 1D Results for a drive beam with density $n_d/n_0 = 0.2$ and length $k_{p0}L_d = 1.9$ and a laser pulse with normalized strength parameter $a_0 = 2.4$, (a) spectrum of laser pulse versus propagation distance, the red curve shows the predicted frequency as determined by equations (1) and (2) and the black line shows the mean frequency, note that the mean frequency increases by a factor of 10, (b) Tapered density profile for dephasingless photon acceleration as determined by equations (1) and (2), (c) drive beam energy in blue and laser pulse energy in red, shown to different scales, the electron drive beam loses energy linearly to the wake and is almost completely depleted of energy, the laser gains about 7% of the initial energy in the drive beam

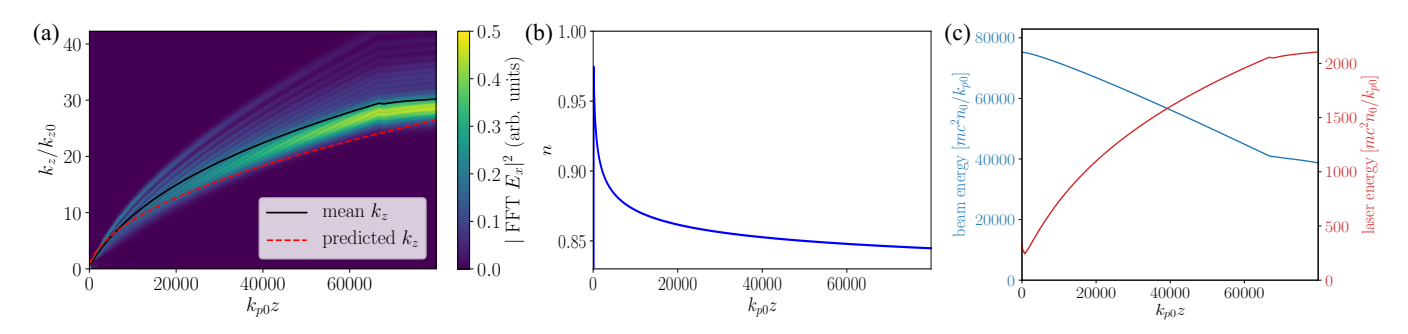


FIG. 4: Results in 1D for drive beam $n_d/n_0 = 0.3$, $k_{p0}L_d = 12.56$ and laser $a_0 = 4.5$, (a) spectrum of laser pulse versus propagation distance, the red curve shows the predicted frequency as determined by equations (1) and (2) and the black line shows the mean frequency, note that mean frequency increases by a factor of 30, (b) Tapered density profile for dephasingless photon acceleration as determined by equations (1) and (2), (c) drive beam energy in blue and laser pulse energy in red, shown to different scales, the electron drive beam loses energy linearly to the wake and loses about half its energy before parts of the beam are depleted and the wake is disrupted. Laser energy increases monotonically, with most of the energy gain occurring early in the simulation.

D. 1D dePWPA with a piecewise approximation to the exact profile

In this section we repeat the previous simulation using a piecewise constant approximation to the tapered plasma density profile. In this case $30\times$ frequency shift and $6\times$ energy gain are still measured, demonstrating that the density profile is robust to perturbations.

The drive beam has density $n_d=0.3n_0$ and length $k_{p0}L_d=12.56$. Initially the laser has $\omega_L=10\omega_{p0}$. The laser has an a_0 of 4.5, with a pulse duration $\omega_{p0}\tau=0.885$, corresponding to an intensity full-width at halfmax (FWHM) of 3 fs when $\lambda_0=800$ nm. We use 30000 cells for 618 cells per λ_{L0} and about 21 cells per λ_{Lf} , a CFL condition of $\omega_{p0}\Delta t=0.9995k_{p0}\Delta x$, and 4 particles per cell.

Figure 5 shows that the mean laser wavenumber matches or exceeds the predicted wavenumber and increases by a factor of more than 30. About 5% of the energy lost by the drive beam is transferred to the witness

laser pulse. The frequency energy transfer sees a discontinuity around $60,000k_{p0}z$. As in the previous section, a portion of the beam is depleted of energy, dephases, loads the wake, and stops the frequency shift of the trailing laser pulse.

This simulation uses a piecewise approximation to the density profile obtained from solving equations (1) and (2). Using a scaling for $100\times$ underdense initial plasma density n_0 relative to an initial laser wavelength of $\lambda_{L0}=800$ nm, the step lengths are 1, 1, 4, 6, 8, 10, and 70 mm. The density over each interval is the density of the numerically evaluated tapered profile at the midpoint of the interval. Significant frequency shift is still obtained, demonstrating that the phase matched photon acceleration scheme is robust to perturbations in the density profile, and could be achieved with a sequence of gas cell targets of increasing length and decreasing plasma density.

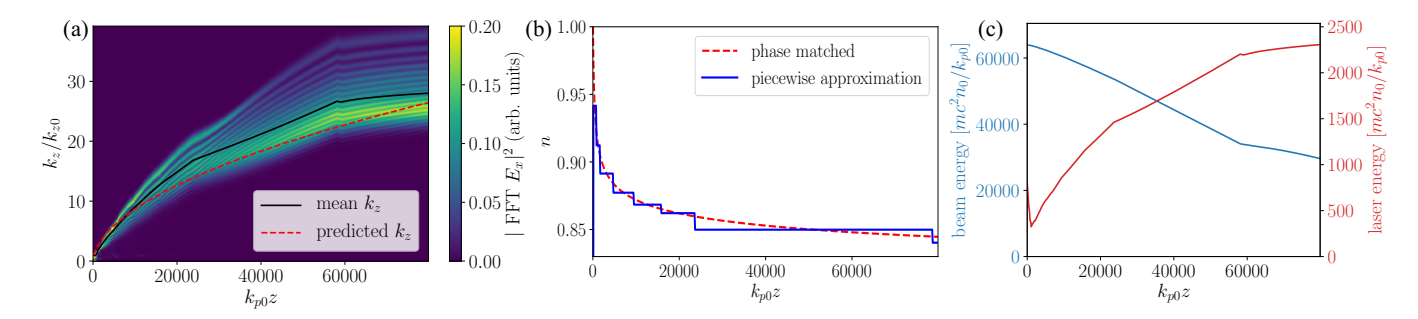


FIG. 5: 1D Results for a drive beam with density $n_d/n_0 = 0.3$, length $k_{p0}L_d = 12.56$ and a laser pulse with normalized strength parameter $a_0 = 4.5$, (a) spectrum of laser pulse versus propagation distance, measured in k_L/k_{L0} where $k_L = k_z$ is the laser wavenumber, the red curve shows the predicted frequency as determined by equations (1) and (2) and the black line shows the mean frequency, note that that mean frequency increases by a factor of 30, (b) Tapered density profile (dashed red) for dephasingless photon acceleration as determined by equations (1) and (2) and piecewise approximation (solid blue), (c) drive beam energy in blue and laser pulse energy in red, shown to different scales, the electron drive beam loses energy linearly to the wake and loses about half its energy before parts of the beam are depleted and the wake is disrupted.

E. 1D long laser pulse

In this section we demonstrate the ability of the model to generate frequency shift even for longer witness laser pulses. As in the preceding two sections, we can see shifts of $30\times$ in frequency, $6\times$ in energy and $25\times$ in intensity. The laser pulse has an initial pulse duration 10 times longer than the previous cases, corresponding to a FWHM duration $\tau_L \approx 28$ fs for $\lambda = 800$ nm light.

The drive beam has density $n_d/n_0=0.3$ and length $k_{p0}L_d=12.56$. The beam has an up-chirp in energy similar to the previous section of the form $\gamma(\omega_{p0}\zeta)=4000+32000(\omega_{p0}\zeta/12.56)$. The chirp helps prevents partial beam depletion but is not optimal; we anticipate that a triangular chirp would be more beneficial. Initially the laser has $\omega_L/\omega_{p0}=10$. The laser has an a_0 of 0.5, with an intensity FWHM of $\omega_{p0}\tau=8$. We use 30000 cells for 618 cells per λ_{L0} and about 21 cells per λ_{Lf} , a CFL condition of $\omega_{p0}\Delta t=0.9995k_{p0}\Delta x$, and 4 particles per cell.

Figure 6 shows that the mean laser wavenumber matches or exceeds the predicted wavenumber and increases by a factor of more than 30. About 5% of the energy lost by the drive beam is transferred to the witness laser pulse. The rate of change in energy transfer has a discontinuity around $60,000k_{p0}z$. This is the drive beam depletion length; at this point a portion of the beam has lost enough energy to move at sub-relativistic velocities and gets caught by the electron-accelerating fields. This loads the wake, so the laser pulse behind no longer sees an increasing density gradient and doesn't experience any more frequency shift. Note that this simulation shows the robustness of the scheme to laser pulse duration.

The reported values of this 1D dimensionless simulation can be understood in physical units if we impose some initial scales. Assuming the initial laser wavelength is 800 nm and the drive beam has an initial root-mean-

square radial extent $\sigma_r=16~\mu\mathrm{m}$, then the system propagates about 10 cm and the shifts are 30× in frequency, from an initial wavelength $\lambda=800~\mathrm{nm}$ to 27 nm, 6× in energy, from $U=50~\mathrm{mJ}$ to 900 nm, 25× in intensity, and 13× in compression, from an initial full-width half-maximum in intensity pulse duration of $c\tau=900~\mathrm{nm}$ to 69 nm.

III. QUASI-3D SIMULATIONS

There are several multi-dimensional effects to consider in applying the density profile derived in 1D for frequency upshift in the 3D case. These include laser pulse diffraction, the transverse wake profile, drive beam self-focusing and the qualitatively different axial density profile in the blowout regime. These affect both the laser pulse dynamics, the electron beam dynamics, and the wake profile.

In one dimension, the region of frequency upshift has length $L \leq \lambda_p/2$ since there is no transverse evolution and so for the entire laser pulse to see frequency upshift, the pulse width must be shorter than $\lambda_p/2$. We note, as did Esarey et al.⁶² that the wake itself has the shape of a plasma channel and can focus a laser pulse. The region of frequency upshift and laser focusing has width $\lambda_p/4$; for frequency upshift and guiding, the pulse width must be less than $\lambda_p/4$. Additionally, for higher intensity pulses above the critical power, relativistic self-focusing can maintain the pulse profile.

In linear theory, the wake profile is the product of the longitudinal and transverse profiles, where the transverse profile of the wake is the transverse profile of the drive beam. Given a drive beam creating a quasilinear wake with a transverse gaussian profile, the wake transverse profile will be gaussian. On axis, the laser pulse sees a parabolic transverse density profile, which, if deep and wide enough, will guide the laser pulse. We use a gaussian

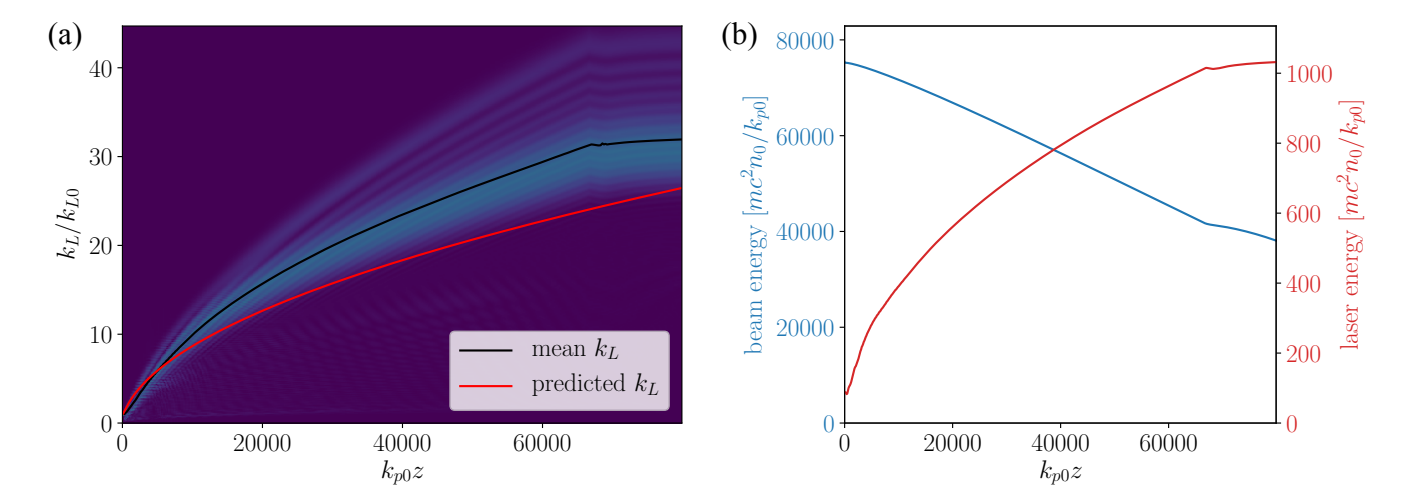


FIG. 6: 1D Results for a drive beam with density $n_d = 0.3$, length $L_d = 12.56$ and a laser pulse with duration $\omega_{p0}\tau_L = 8$ and normalized strength parameter $a_0 = 0.5$, corresponding to 28 fs for 800 nm light and initial plasma density $n_0 = 1.74 \times 10^{19} \text{cm}^{-3}$, (a) spectrum of laser pulse versus propagation distance, measured in k_L/k_{L0} where $k_L = k_z$ is the laser wavenumber, the dashed red curve shows the predicted frequency as determined by equations (1) and (2) and the black line shows the mean frequency, note that that mean frequency still increases by a factor of 30, (b) drive beam energy in blue and laser pulse energy in red, shown to different scales, the electron drive beam loses energy linearly to the wake and loses about half its energy before parts of the beam are depleted and the wake is disrupted. Note that frequency shift and energy gain are similar to the initially single cycle case presented in Fig. 4.

drive electron beam and find that the laser pulse stays focused over more than 100 Rayleigh ranges. We have not experienced issues with focusing effects with the witness laser.

The drive beam, however, is limited by focusing effects in 3D. The most substantial issue is that the tail of the electron drive beam experiences radial focusing forces in the wake created by the drive beam and is pinched. Once the beam radius decreases below a threshold value, the wake develops the quasi-spherical shape characteristic of the blowout regime, a regime distinct to 2- and 3-dimensions. In the blowout regime, the longitudinal wake profile becomes singular and the region with a density gradient becomes vanishingly small with slope tending to infinity. The laser pulse no longer fits in the region of frequency upshifting and so the blowout wake regime is to be avoided. Even if the drive beam is initially broad and creates an almost 1D wake, in simulations the beam can be pinched until it creates a wake in the blowout regime. This is a significant effect that is detrimental to the current frequency shifting scheme for long drive beams and finding ways—other than using an ultrashort beam—to mitigate this effect is active research.

A. 3D dePWPA with short broad drive beam

We use the PIC code $FBPIC^{80}$ to study dePWPA in a quasi-3D geometry. FBPIC runs on GPUs. The advantage to FBPIC is its spectral cylindrical representation. The spectral field solve reduces numerical dispersion with

fewer grid points than the standard Yee finite difference scheme. The spectral cylindrical representation decomposes the azimuthal direction into a Fourier representation. Our problem is nearly cylindrically symmetric, with the most significant asymmetry in the linear polarization of the laser. We use two angular modes, which is enough to capture the linearly polarized laser as well as the cylindrically symmetric wake from the drive beam.

We use the quasi-3D particle-in-cell code FBPIC⁸⁰ to demonstrate the dePWPA scheme. For the 3D results we list physical quantities in SI units rather than the normalized units presented earlier. In the simulation, the drive electron beam has a charge Q = 8.6 pC, length $c\tau = 0.4 \ \mu m$, focused radial extent $\sigma_r = 32 \ \mu m$, and a divergence $\sigma_{r'} = 0.4$ mrad. The beam has a linear upchirp of the form $\gamma(\zeta) = 5 \times 10^4 + 5 \times 10^4 (c\zeta/L_d)$ for an average beam particle energy of 50 GeV. The chirp mitigates beam erosion somewhat but there is room for tuning. The beam parameters are similar to those accessible at the SLAC FACET-II facility $^{81}.$ The laser has a normal statement of 12 malized field strength parameter $a_0 = 1$ and initial wavelength $\lambda_{L0} = 800$ nm, corresponding to a peak intensity $I=2.1\times 10^{18}~{\rm Wcm}^{-2}$, a pulse width $c\tau=1.25~\mu{\rm m}$, and a spot size of $w_0=2\lambda_{p0}=20\lambda_{L0}=16~\mu{\rm m}$, starting with its centroid $\zeta_{\rm cent} = 6.6 \ \mu \rm m/c$ behind the front of the electron drive beam. For these parameters, $\zeta_{\delta} = 5.4 \ \mu \text{m/c}$, so we see some robustness to variation in initial position of the laser pulse. Single cycle laser pulses at this intensity have been demonstrated experimentally⁷³. Visualization of the drive beam, its wake and the witness laser pulse in the quasi-3D simulation is shown in Fig. 7.

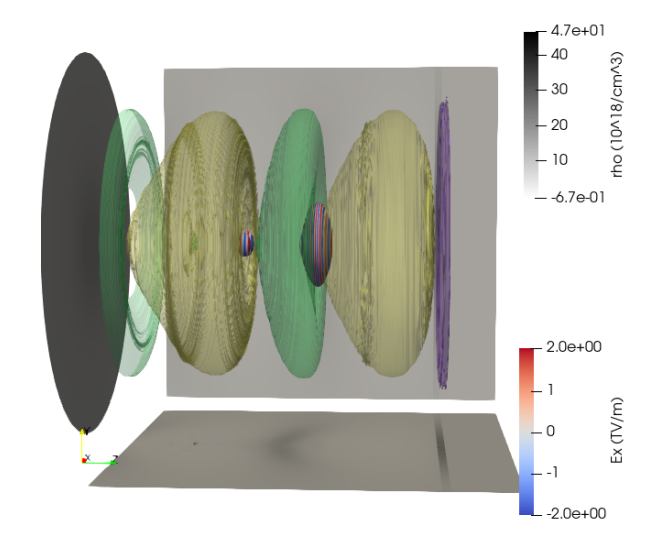


FIG. 7: Isocontours from quasi-3D simulation data demonstrating phase matched photon acceleration; the purple disk at the right is the drive electron beam, yellow and green are the positive and negative density perturbations of the wake, and the blue and red spheroid is a contour of the envelope of the transverse electric field, colored to show the laser pulse field phase.

We use the plasma density profile shown in Fig. 8 and determined through a numerical algorithm⁷⁷ from equations 1 and 2, scaled by $n_0 = 1.74 \times 10^{19} \ \mathrm{cm^{-3}}$, which is $100 \times$ less than the initial critical density of the laser. For numerical parameters we use 3200×200 grid points and 2 angular modes. This gives 85 cells per λ_{L0} and about 8 cells per λ_{Lf} , which therefore requires a dispersion-free solver or numerical dispersion would be an impediment. For the plasma we use 2×2 particles per cell (ppc) in the z and r directions times 8 ppc in the azimuthal direction.

The results of the quasi-3D simulation of PMPA can be seen in Fig. 9. Figure (a) shows the spectrum as a function of length propagated in the simulation. Overlaid is the theoretical model of Eqns. (1) and (2) (red line, identical to the analytic predictions of equations, which predicts the shift of the photons well. Figure (b) shows the initial spectrum and the spectrum at the end of the simulation. As well as showing that the pulse maintains a narrow bandwidth, the amplitude of the spectrum has increased, indicating the energy of the laser pulse increased. Figure (c) shows the energy evolution of the drive beam and the laser pulse. The drive beam loses 25 J of energy over the course of the simulation while the laser pulse, initially having 50 mJ, gains 200 mJ for about 1% energy transfer efficiency, which could be increased by optimization of the driver. Note that overall pulse energy gain is not unexpected, as to within the quasistatic approximation, local field action is conserved⁸², and so the energy gain by the pulse would be expected to scale with the frequency increase. In the simulations, the nearly $10\times$ frequency shift results in a lower 5× pulse energy gain,

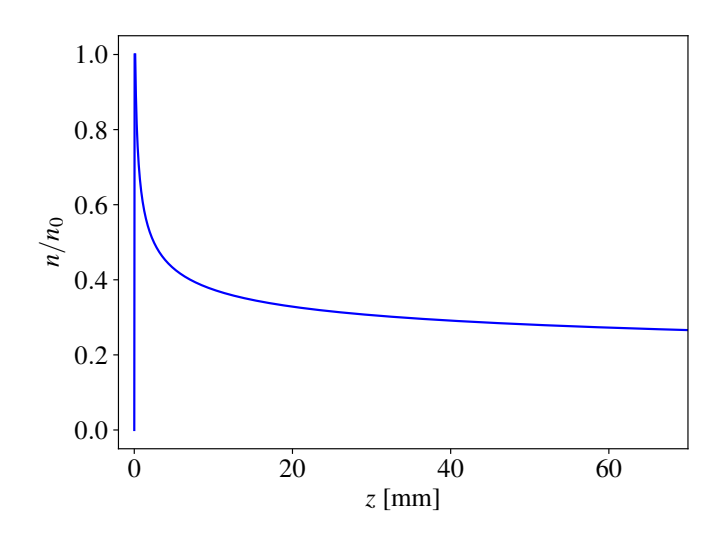


FIG. 8: Density profile for unlimited photon acceleration driven by an ultrashort driver with $A = (k_{p0}L_{d0})(n_{d0}/n_0) = 0.38$.

because of losses due to diffraction/dispersion.

Due to the nonlinear wake, the back of the pulse sees a steeper plasma gradient than the front of the pulse. The pulse develops significant up-chirp, which, together with dispersion, leads to a $2.7\times$ compression of the pulse from an initial duration of $c\tau=1.25~\mu\mathrm{m}$ to $0.51~\mu\mathrm{m}$. The intensity sees a significant increase of $20\times$ from an initial intensity $I=2\times10^{18}~\mathrm{W/cm^2}$ to $4\times10^{19}~\mathrm{W/cm^2}$, a relativistic intensity corresponding to $a_0=0.4$ at 80 nm.

We note that the laser pulse stays focused throughout the course of the simulation. The drive beam has a gaussian radial profile, which is therefore parabolic close to axis. Thus the wake has an approximately parabolic transverse profile and acts as a guiding channel for the laser pulse. The pulse stays focused over more than 10 centimeters when the Rayleigh range corresponding to the final wavelength is $z_R = \pi w_0^2/\lambda_{Lf} \approx 10$ mm, meaning that the pulse was effectively guided for more than 10 Rayleigh lengths.

The data ends at z=72 mm. Beyond this length, the beam driver has lost sufficient energy to break up. Going beyond this length would also start to reach the resolution limit of the simulation for the maximum frequency. In 1D simulations at higher resolution with a longer drive pulse, where tuning of the drive beam propagation was easier through parametric studies of many simulations, we have demonstrated even $30\times$ frequency shifts. Beginning with the 2nd harmonic of a Ti:Sapph laser at 400 nm, a 30 times shift (scaling the plasma / initial conditions to maintain similarity and fixing a_0) would result in 125 mJ pulses of coherent 13.3 nm light, which may be useful for photolithography.

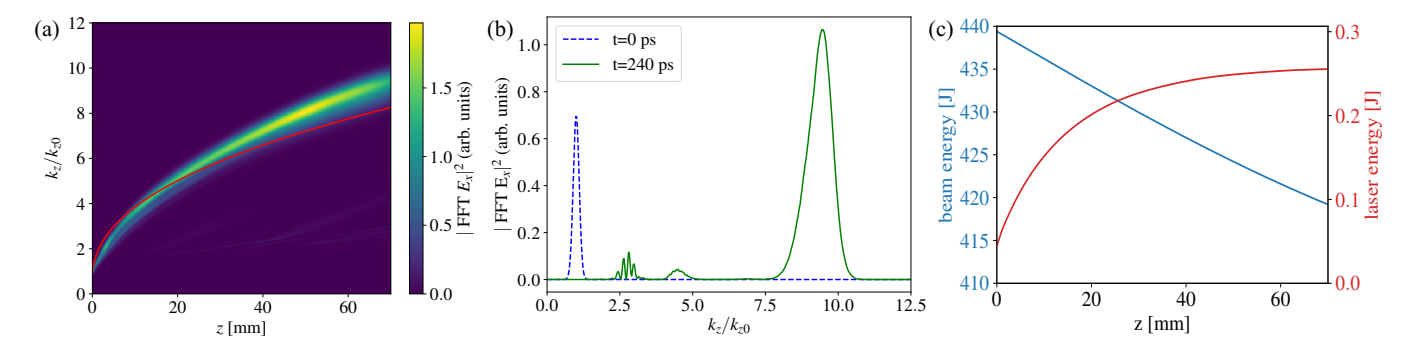


FIG. 9: Quasi-3D simulation results from FBPIC for a drive beam with $k_{p0}L_{d0} = 0.5$. (a) Comparing the initial and final spectra. The spectrum has shifted to about $10\times$ the initial wavenumber. (b) Plot of the spectrum over time. The red line is the theoretical 1D frequency shift. (c) Drive beam energy (blue) and witness laser energy (red)

B. Quasi-3D simulation with piecewise density profile

In this section we repeat the simulation of the previous section but use a piecewise-constant approximation to the density profile, as shown in figure 10. We still find $10\times$ frequency shift and $5\times$ energy gain, demonstrating that the tapered density profile is robust to imperfections or variations from ideal in plasma density provided that it follows the ideal profile on average.

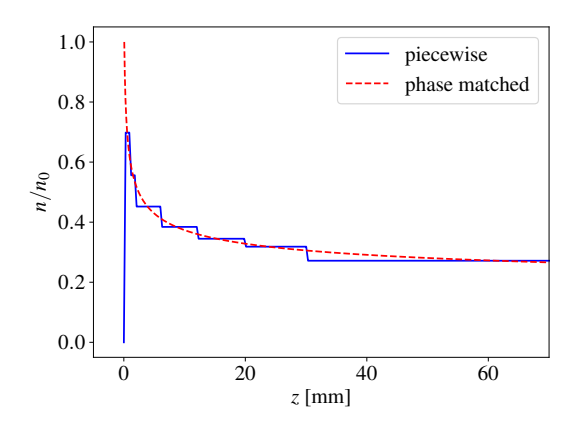


FIG. 10: Piecewise approximation to the profile used for quasi-3D simulation

The approximation is made on progressively longer intervals, as in the previous 1D piecewise simulation. The first two steps are each 1 mm long, then 4 mm, 6 mm, 8 mm, 10 mm, and the last step here is 70 mm long. The density over each interval is the density of the numerically evaluated tapered profile at the midpoint of the interval.

We can see the results of propagating through the piecewise constant approximation to the phase matched density profile in figure 11. Similarly to the simulation with the phase matched density profile, in part (a) we see that the final frequency is almost 10 times the initial frequency, and the amplitude of the spectrum has increased, indicating the energy of the laser pulse increased. The

frequency shift is shown over the course of the simulation in (b), following the theoretical prediction indicated by the red line. The center of the distribution follows the theoretical prediction.

In figure 9(c) we see the loss of drive beam energy is linear with propagation distance, as the beam energy is continuously transferred to the wake. On the other hand, the laser gains about 200 mJ for a $5\times$ shift in energy. For this simulation about 1% of the energy lost by the drive beam to the wake was transferred to the laser pulse.

Comparing the piecewise results in figure 11 with the results using the exact tapered profile 9, we see similar frequency shifts and energy gains. We see slightly more shift in the exact case, where the center of the spectrum is above the predicted frequency, than in the piecewise case, where the center of the spectrum is close to the predicted frequency. We also see in the late-time spectra plots in figures 11(a) and 11(b) that the amplitude of the the spectrum is slightly lower in the piecewise case, and in figures 11(c) and 11(c) that the energy gain of the laser pulse is slightly less. These discrepancies are slight and speak strongly to the reliability of the tapered density profile for attaining frequency shift.

IV. CONCLUSIONS AND FUTURE DIRECTIONS

In summary, we have demonstrated a scheme for large frequency upshift of a laser pulse using the wake generated by a relativistic particle beam propagating through a tapered plasma density profile. Our analytic model predicts arbitrary frequency shift limited only by the drive beam. We demonstrate the model in several 1- and quasi-3D simulations. These demonstrate how quickly a laser dephases in the wake if the phase-matched density profile is not used. 1D simulations show frequency shifts of $30\times$ or more if a sufficient drive beam is used, as well as demonstrating that drive beams of arbitrary length and density can be used and that non-ideal, physically realizable density profiles still lead to $30\times$ frequency shifts. An important feature of the beam-driven photon-

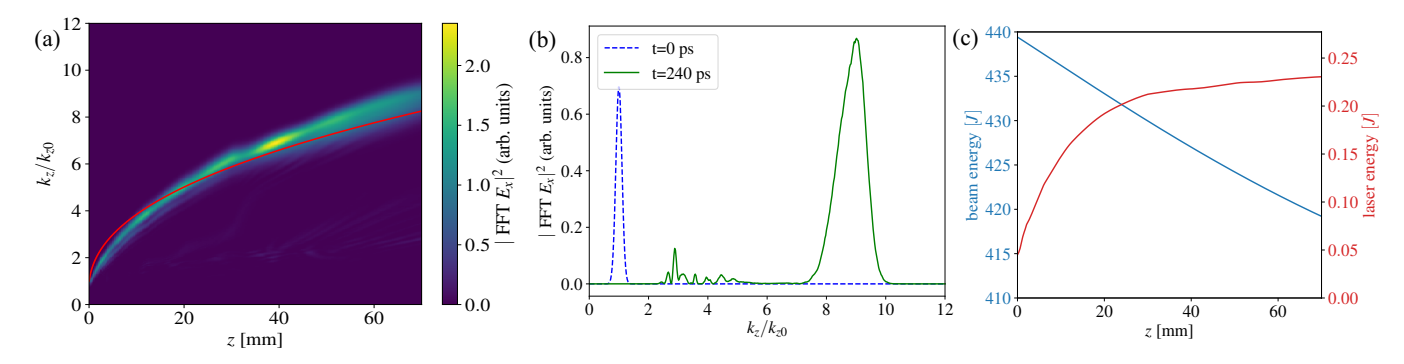


FIG. 11: Quasi-3D simulation results from FBPIC for a drive beam with $k_{p0}L_{d0} = 0.5$ using a piecewise approximation to the phase matched density profile. (a) Comparing the initial and late-time (z = 72 mm) spectra. The spectrum has shifted to almost 10x the initial wavenumber. (b) Plot of the spectrum over time. The red line is the theoretical 1D frequency shift. (c) Drive beam energy (blue) and witness laser energy (red)

acceleration scheme is its robustness. In the simulations explored here, in addition to 3D effects, longer pulses and non-ideal plasma conditions did not substantially degrade performance. Although the analytic work was derived assuming a weak and extremely short witness pulse, longer, $\omega_p \tau > 1$, and more intense, $a_0 > 1$, pulses still resulted in large frequency shifts and high efficiency but with additional spectral broadening, mostly because of the initial trapping of the light.

In the quasi-3D simulations shown here, an short, unoptimized driver was used, but in principle there is much scope for increasing coupling of driver energy to the wake/witness laser pulse, including advancements in spatiotemporally evolving electron beam drivers⁸³. Quasi-3D simulation results directly demonstrated a 10× frequency shift with 1% energy transfer efficiency. Guiding of the laser pulse is achieved by the wake itself, in addition to the lengthening of the Rayleigh range as the frequency increases and possibly relativistic self-focusing. In quasi-3D simulations we have also demonstrated the robustness of the plasma density profile to perturbations, as well as a route to practical realization of the tapered density profile, using a piecewise constant approximation to the density profile. Frequency shifts of $10\times$ are still observed in quasi-3D simulations with a non-ideal profile.

The overall energy amplification of the witness laser pulse is another notable feature of the scheme. Previous authors have shown that under certain assumptions "photon number" (or more precisely, classical action) is conserved in fully ionized plasma wakes 62,82,84 . In our simulations, in 1D the overall pulse energy scales precisely proportional to the average frequency shift, consistent with this conclusion (i.e $U_{\rm pulse} \propto \langle \omega \rangle$). In 3D, this relationship does not exactly hold in the simulations, which in part could be because of diffraction of some pulse energy out of the wake in addition to slight spatial non-uniformity of the frequency shift.

Our results indicate that using an electron beam driver is a viable route to generate high-power, high-frequency coherent radiation. It may also be possible to demonstrate these shifts with a laser beam driver, although dispersion and frequency shifting of the lead pulse require compensation.

To evaluate the prospects of this scheme for attaining greater frequency shifts, we consider the relation for frequency gain as a function of plasma density derived in $\operatorname{Ref.}^{75}$,

$$\omega(n) = \omega_0 \exp\left[A\left(\zeta_\delta(n) - \zeta_{\delta 0}\right)\right] \,, \tag{4}$$

defined for n in $(0, n_0]$ where $n(0) = n_0$ and where ω_0 and $\zeta_{\delta 0}$ are the initial frequency position in the wake of the witness pulse respectively. In figure 12 we plot several curves indicating how the frequency shift as the laser propagates through decreasing plasma density are given for drive beams of charge Q = 1, 2, and 5 nC, corresponding to amplitudes A = 0.18, 0.35, and 0.88.We can see that the strong drive sees greater frequency shifts for the same change in plasma density. Several points are marked on each trajectory indicating how far the laser and drive beam must propagate to reach that frequency-density point on the trajectory, if the initial laser pulse has wavelength $\lambda = 800 \ \mu m$ and the initial plasma density is $n_0 = 1.7 \times 10^{19}$ cm⁻¹. For a drive beam with Q = 5 nC, the model predicts $100 \times$ frequency shift in 2 m of propagation. On the other hand, for a drive beam with Q = 1 nC a frequency shift of $100 \times$ would require 1 km of propagation. One fundamental limitation on the breakdown of the continuum approximation for the plasma and how this potentially restricts the frequency shift through the onset of scattering from individual plasma electrons. This is left for future investigation. The enhanced shifts with higher drive beam amplitude and more nonlinear wakes show the need for the nonlinear model derived in this paper and the need to pursue higher-amplitude drivers in subsequent research.

We envision three broad directions for the investigating the future of unlimited photon acceleration. First, understanding 3D transverse effects and feasible acceleration with finite-duration electron beams. Second, optimization of electron beam, laser beam, and plasma density

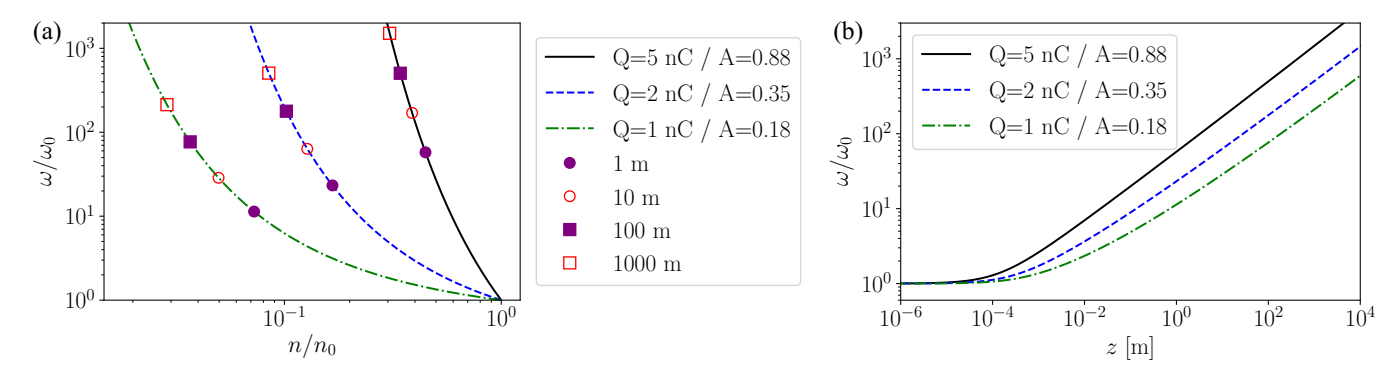


FIG. 12: (a) Relative frequency gain as a function of density, $(\omega/\omega_0)(n)$, is plotted for beam drive charges Q = 1 nC, 2 nC, and 5 nC. The frequency gain-density curves are labeled with markers indicating the distance that the laser and drive beam must propagate to achieve the indicated shift. (b) Relative frequency gain as a function of z in meters, plotted for beam drive charges Q = 1 nC, 2 nC, and 5 nC.

profile. Third, developing the phase matched system of equations for laser-driven photon acceleration.

The evolution of the drive beam has a significant effect on the wake profile. In particular, the radial focusing forces of the wake cause the drive beam to pinch. A drive beam that is initially broad enough for the 1D wake expressions to be valid will shrink until radial effects change the plasma wavelength and ultimately the highly nonlinear blowout regime is reached, which is undesirable for photon acceleration.

Several open questions remain with regards to understanding and controlling the transverse drive beam dynamics and their effects on photon acceleration. First, while we have avoided the blowout regime in pursuit of finite duration plasma gradients, it may be possible to realize frequency shifts within the blowout regime. If not, then it is necessary to avoid the blowout regime somehow. Perhaps there are matching conditions so that the electron beam propagates without self-focusing into a blowout-producing profile. It may be that a gaussian beam will self-focus too strongly, but perhaps beams can be constructed having a higher divergence at the back of the beam and so not self-focusing before the depletion length is reached.

Also, we use simple expressions for the index of refraction and laser group velocity. Several nonlinear effects were neglected in the analysis, including relativistic, intensity and channel effects on the wake profile and laser evolution. The effects of these corrections are unknown but could be large enough to affect the wake or laser pulse.

The next broad category of future directions is in optimizing the frequency shift and efficiency of our scheme. As in electron acceleration^{85,86}, we anticipate that a properly shaped laser pulse should admit laser beam loading of the wake. This could enhance energy gain, frequency shift, or the amount of light we can shift. Also, in this work we used very short, single cycle laser pulses. While such pulses have been experimentally demonstrated⁷³, as the simulations demonstrated, the

scheme isn't restricted to single cycle pulses.

The third category of future directions is laser-driven photon acceleration. Laser-driven photon acceleration has been studied more than electron-beam-driven photon acceleration but not with a profile such as we have developed here. In this case, the frequency-shifting pulse would have a higher group velocity than the drive pulse and so would eventually catch up to the drive pulse. This limits how long and how much the frequency can be increased. There have been theoretical investigations ⁶³ into laser-driven frequency upshift but little successful simulation and even less on a dephasingless frequency upshift.

ACKNOWLEDGMENTS

This work was supported by AFOSR grant FA9550-19-1-0072. Computational resources were provided by Advanced Research Computing at the University of Michigan. The authors would like to acknowledge the OSIRIS Consortium, consisting of UCLA and IST (Lisbon, Portugal) for providing access to the OSIRIS 4.0 framework.

⁴⁴ J. Rossbach, J. R. Schneider, and W. Wurth, 10 years of pioneering x-ray science at the free-electron laser flash at desy, Physics Reports 808, 1–74 (2019), 10 years of pioneering X-ray science at the Free-Electron Laser FLASH at DESY.

⁴⁵M. A. Khokhlova and V. V. Strelkov, Highly efficient XUV generation via high-order frequency mixing, New Journal of Physics 22, 093030 (2020).

⁴⁶Z. Chang, A. Rundquist, H. Wang, M. M. Murnane, and H. C. Kapteyn, Generation of coherent soft x rays at 2.7 nm using high harmonics, Phys. Rev. Lett. **79**, 2967–2970 (1997).

⁴⁷S. V. Bulanov, T. Esirkepov, and T. Tajima, Light intensification towards the schwinger limit, Phys. Rev. Lett. 91, 085001–085004 (2003).

⁴⁸M. Kando, A. S. Pirozhkov, K. Kawase, T. Z. Esirkepov, Y. Fukuda, H. Kiriyama, H. Okada, I. Daito, T. Kameshima, Y. Hayashi, H. Kotaki, M. Mori, J. K. Koga, H. Daido, A. Y. Faenov, T. Pikuz, J. Ma, L. M. Chen, E. N. Ragozin, T. Kawachi, Y. Kato, T. Tajima, and S. V. Bulanov, Enhancement of photon number reflected by the relativistic flying mirror, Phys. Rev. Lett. 103, 235003–235007 (2009).

- ⁴⁹S. V. Bulanov, T. Z. Esirkepov, and M. Kando, Relativistic mirrors in plasmas. novel results and perspectives, Physics-Uspekhi **56** (2013), 10.3367/UFNe.0183.201305a.0449.
- ⁵⁰B. R. Benware, C. D. Macchietto, C. H. Moreno, and J. J. Rocca, Demonstration of a high average power tabletop soft x-ray laser, Phys. Rev. Lett. 81, 5804–5807 (1998).
- ⁵¹S. C. Wilks, J. M. Dawson, W. B. Mori, T. Katsouleas, and M. E. Jones, Photon accelerator, noop Physical Review Letters 62 (1989).
- ⁵²S. Weinberg, Eikonal Method in Magnetohydrodynamics, Physical Review **126**, 1899–1909 (1962).
- ⁵³ J. T. Mendonca, noop Theory of photon acceleration (Institute of Physics Pub, 2001).
- ⁵⁴E. Esarey, G. Joyce, and P. Sprangle, Frequency up-shifting of laser pulses by copropagating ionization fronts, Physical Review A 44, 3908–3911 (1991).
- ⁵⁵L. Oliveira e Silva and J. T. Mendonca, Photon acceleration in superluminous and accelerated ionization fronts, IEEE Transactions on Plasma Science 24, 316–322 (1996).
- ⁵⁶M. R. Shcherbakov, K. Werner, Z. Fan, N. Talisa, E. Chowdhury, and G. Shvets, Photon acceleration and tunable broadband harmonics generation in nonlinear time-dependent metasurfaces, Nature Communications 10, 1345 (2019).
- ⁵⁷J. M. Dias, C. Stenz, N. Lopes, X. Badiche, F. Blasco, A. Dos Santos, L. Oliveira e Silva, A. Mysyrowicz, A. Antonetti, and J. T. Mendonça, Experimental evidence of photon acceleration of ultrashort laser pulses in relativistic ionization fronts, Phys. Rev. Lett. **78**, 4773–4776 (1997).

⁵⁸C. W. Siders, S. P. Le Blanc, D. Fisher, T. Tajima, M. C. Downer, A. Babine, A. Stepanov, and A. Sergeev, Laser wakefield excitation and measurement by femtosecond longitudinal interferometry, Phys. Rev. Lett. **76**, 3570–3573 (1996).

- ⁵⁹C. D. Murphy, R. Trines, J. Vieira, A. J. W. Reitsma, R. Bingham, J. L. Collier, E. J. Divall, P. S. Foster, C. J. Hooker, A. J. Langley, P. A. Norreys, R. A. Fonseca, F. Fiuza, L. O. Silva, J. T. Mendonça, W. B. Mori, J. G. Gallacher, R. Viskup, D. A. Jaroszynski, S. P. D. Mangles, A. G. R. Thomas, K. Krushelnick, and Z. Najmudin, Evidence of photon acceleration by laser wake fields, Physics of Plasmas 13, 033108 (2006).
- ⁶⁰M. R. Edwards, K. Qu, Q. Jia, J. M. Mikhailova, and N. J. Fisch, Cascaded chirped photon acceleration for efficient frequency conversion, noop Physics of Plasmas 25 (2018).
- 61 Z. Nie, C. H. Pai, J. Hua, C. Zhang, Y. Wu, Y. Wan, F. Li, J. Zhang, Z. Cheng, Q. Su, S. Liu, Y. Ma, X. Ning, Y. He, W. Lu, H. H. Chu, J. Wang, W. B. Mori, and C. Joshi, Relativistic single-cycle tunable infrared pulses generated from a tailored plasma density structure, Nature Photonics 12, 489–494 (2018).
- ⁶²E. Esarey, A. Ting, and P. Sprangle, Frequency shifts induced in laser pulses by plasma waves, Physical Review A 42, 3526–3531 (1990).
- ⁶³V. A. Mironov, A. M. Sergeev, E. V. Vanin, G. Brodin, and J. Lundberg, Upper limits for frequency up-conversion in the nonlinear photon accelerator, Physical Review A 46, R6178–R6180 (1992).
- ⁶⁴S. V. Bulanov, V. I. Kirsanov, F. Pegoraro, and A. S. Sakharov, Charged particle and photon acceleration by wake field plasma waves in nonuniform plasmas, noop Laser Physics 3, 1078–1087 (1993).
- ⁶⁵A. J. Howard, D. Turnbull, A. S. Davies, P. Franke, D. H. Froula, and J. P. Palastro, Photon Acceleration in a Flying Focus, Physical Review Letters 123, 124801 (2019).
- ⁶⁶J. P. Palastro, J. L. Shaw, P. Franke, D. Ramsey, T. T. Simpson, and D. H. Froula, Dephasingless laser wakefield acceleration, Phys. Rev. Lett. **124**, 134802 (2020).
- ⁶⁷A. Debus, R. Pausch, A. Huebl, K. Steiniger, R. Widera, T. E. Cowan, U. Schramm, and M. Bussmann, Circumventing the Dephasing and Depletion Limits of Laser-Wakefield Acceleration, noop Physical Review X 9 (2019).

- ⁶⁸C. Caizergues, S. Smartsev, V. Malka, and C. Thaury, Phase-locked laser-wakefield electron acceleration, Nature Photonics 14, 475–479 (2020).
- ⁶⁹S. V. Bulanov, V. A. Vshivkov, G. I. Dudnikova, N. M. Naumova, F. Pegoraro, and I. V. Pogorelsky, Laser acceleration of charged particles in inhomogeneous plasmas i, *Plasma Physics Reports*, 23, 259–269 (1997).
- ⁷⁰P. Sprangle, B. Hafizi, J. R. Peñano, R. F. Hubbard, A. Ting, C. I. Moore, D. F. Gordon, A. Zigler, D. Kaganovich, and T. M. Antonsen, Wakefield generation and GeV acceleration in tapered plasma channels, Physical Review E 63, 056405 (2001).
- ⁷¹E. Guillaume, A. Döpp, C. Thaury, K. Ta Phuoc, A. Lifschitz, G. Grittani, J.-P. Goddet, A. Tafzi, S. Chou, L. Veisz, and V. Malka, Electron Rephasing in a Laser-Wakefield Accelerator, Physical Review Letters 115, 155002 (2015).
- ⁷²S. V. Bulanov, T. Z. Esirkepov, Y. Hayashi, H. Kiriyama, J. K. Koga, H. Kotaki, M. Mori, and M. Kando, On some theoretical problems of laser wake-field accelerators, Journal of Plasma Physics 82, 905820308 (2016).
- ⁷³D. Guénot, D. Gustas, A. Vernier, B. Beaurepaire, F. Böhle, M. Bocoum, M. Lozano, A. Jullien, R. Lopez-Martens, A. Lifschitz, and J. Faure, Relativistic electron beams driven by kHz single-cycle light pulses, Nature Photonics 11, 293–296 (2017).
- ⁷⁴J. Kim, V. L. J. Phung, K. Roh, M. Kim, K. Kang, and H. Suk, Development of a density-tapered capillary gas cell for laser wakefield acceleration, Review of Scientific Instruments 92, 023511 (2021).
- ⁷⁵R. T. Sandberg and A. G. R. Thomas, Photon acceleration from optical to xuv, Phys. Rev. Lett. **130** (2023), 10.1103/Phys-RevLett.130.085001.
- ⁷⁶J. B. Rosenzweig, Nonlinear plasma dynamics in the plasma wake-field accelerator, Physical Review Letters **58**, 555–558 (1987).
- ⁷⁷R. T. Sandberg and A. G. R. Thomas, Dephasingless plasma wakefield photon acceleration, noop In preparation.
- ⁷⁸R. G. Hemker, Particle-in-Cell Modeling of Plasma-Based Accelerators in Two and Three Dimensions, noop Ph.D. thesis, UCLA (1999).
- ⁷⁹R. A. Fonseca, L. O. Silva, F. S. Tsung, V. K. Decyk, W. Lu, C. Ren, W. B. Mori, S. Deng, S. Lee, T. Katsouleas, and J. C. Adam, Osiris: A three-dimensional, fully relativistic particle in cell code for modeling plasma based accelerators, in noop *Computational Science ICCS 2002*, edited by P. M. A. Sloot, A. G. Hoekstra, C. J. K. Tan, and J. J. Dongarra (Springer Berlin Heidelberg, Berlin, Heidelberg, 2002) pp. 342–351.
- ⁸⁰R. Lehe, M. Kirchen, I. A. Andriyash, B. B. Godfrey, and J. L. Vay, A spectral, quasi-cylindrical and dispersion-free Particle-In-Cell algorithm, Computer Physics Communications 203, 66–82 (2016).
- ⁸¹V. Yakimenko, L. Alsberg, E. Bong, G. Bouchard, C. Clarke, C. Emma, S. Green, C. Hast, M. Hogan, J. Seabury, N. Lipkowitz, B. O'Shea, D. Storey, G. White, and G. Yocky, FACET-II facility for advanced accelerator experimental tests, Physical Review Accelerators and Beams 22, 101301 (2019).
- ⁸²W. Mori, The physics of the nonlinear optics of plasmas at relativistic intensities for short-pulse lasers, IEEE Journal of Quantum Electronics 33, 1942–1953 (1997).
- 83 F. Li, T. N. Dalichaouch, J. R. Pierce, X. Xu, F. S. Tsung, W. Lu, C. Joshi, and W. B. Mori, noop Ultra-bright electron bunch injection in a plasma wakefield driven by a superluminal flying focus electron beam, (2021), http://arxiv.org/abs/2108.00030 arXiv:2108.00030 [physics.plasm-ph].
- ⁸⁴L. Oliveira e Silva and J. T. Mendonça, Kinetic theory of photon acceleration: Time-dependent spectral evolution of ultrashort laser pulses, Phys. Rev. E 57, 3423–3431 (1998).
- ⁸⁵T. Katsouleas, S. Wilks, P. Chen, J. M. Dawson, and J. J. Su, Beam loading in plasma accelerators, noop Particle

- Accelerators 22, 81–99 (1987).
- ⁸⁶M. Tzoufras, W. Lu, F. S. Tsung, C. Huang, W. B. Mori, T. Katsouleas, J. Vieira, R. A. Fonseca, and L. O. Silva, Beam loading by electrons in nonlinear plasma wakes, Physics of Plasmas 16, 056705 (2009).
- ⁴⁴J. Rossbach, J. R. Schneider, and W. Wurth, "10 years of pioneering x-ray science at the free-electron laser flash at desy," Physics Reports 808, 1–74 (2019), 10 years of pioneering X-ray science at the Free-Electron Laser FLASH at DESY.
- ⁴⁵M. A. Khokhlova and V. V. Strelkov, "Highly efficient XUV generation via high-order frequency mixing," New Journal of Physics 22, 093030 (2020).
- ⁴⁶Z. Chang, A. Rundquist, H. Wang, M. M. Murnane, and H. C. Kapteyn, "Generation of coherent soft x rays at 2.7 nm using high harmonics," Phys. Rev. Lett. **79**, 2967–2970 (1997).
- ⁴⁷S. V. Bulanov, T. Esirkepov, and T. Tajima, "Light intensification towards the schwinger limit," Phys. Rev. Lett. **91**, 085001–085004 (2003).
- ⁴⁸M. Kando, A. S. Pirozhkov, K. Kawase, T. Z. Esirkepov, Y. Fukuda, H. Kiriyama, H. Okada, I. Daito, T. Kameshima, Y. Hayashi, H. Kotaki, M. Mori, J. K. Koga, H. Daido, A. Y. Faenov, T. Pikuz, J. Ma, L. M. Chen, E. N. Ragozin, T. Kawachi, Y. Kato, T. Tajima, and S. V. Bulanov, "Enhancement of photon number reflected by the relativistic flying mirror," Phys. Rev. Lett. 103, 235003–235007 (2009).
- ⁴⁹S. V. Bulanov, T. Z. Esirkepov, and M. Kando, "Relativistic mirrors in plasmas. novel results and perspectives," Physics-Uspekhi 56 (2013), 10.3367/UFNe.0183.201305a.0449.
- ⁵⁰B. R. Benware, C. D. Macchietto, C. H. Moreno, and J. J. Rocca, "Demonstration of a high average power tabletop soft x-ray laser," Phys. Rev. Lett. 81, 5804–5807 (1998).
- ⁵¹S. C. Wilks, J. M. Dawson, W. B. Mori, T. Katsouleas, and M. E. Jones, "Photon accelerator," Physical Review Letters **62** (1989).
- ⁵²S. Weinberg, "Eikonal Method in Magnetohydrodynamics," Physical Review **126**, 1899–1909 (1962).
- ⁵³J. T. Mendonca, *Theory of photon acceleration* (Institute of Physics Pub, 2001).
- ⁵⁴E. Esarey, G. Joyce, and P. Sprangle, "Frequency up-shifting of laser pulses by copropagating ionization fronts," Physical Review A 44, 3908–3911 (1991).
- ⁵⁵L. Oliveira e Silva and J. T. Mendonca, "Photon acceleration in superluminous and accelerated ionization fronts," IEEE Transactions on Plasma Science 24, 316–322 (1996).
- ⁵⁶M. R. Shcherbakov, K. Werner, Z. Fan, N. Talisa, E. Chowdhury, and G. Shvets, "Photon acceleration and tunable broadband harmonics generation in nonlinear time-dependent metasurfaces," Nature Communications 10, 1345 (2019).
- ⁵⁷J. M. Dias, C. Stenz, N. Lopes, X. Badiche, F. Blasco, A. Dos Santos, L. Oliveira e Silva, A. Mysyrowicz, A. Antonetti, and J. T. Mendonça, "Experimental evidence of photon acceleration of ultrashort laser pulses in relativistic ionization fronts," Phys. Rev. Lett. 78, 4773–4776 (1997).
- ⁵⁸C. W. Siders, S. P. Le Blanc, D. Fisher, T. Tajima, M. C. Downer, A. Babine, A. Stepanov, and A. Sergeev, "Laser wakefield excitation and measurement by femtosecond longitudinal interferometry," Phys. Rev. Lett. **76**, 3570–3573 (1996).
- ⁵⁹C. D. Murphy, R. Trines, J. Vieira, A. J. W. Reitsma, R. Bingham, J. L. Collier, E. J. Divall, P. S. Foster, C. J. Hooker, A. J. Langley, P. A. Norreys, R. A. Fonseca, F. Fiuza, L. O. Silva, J. T. Mendonça, W. B. Mori, J. G. Gallacher, R. Viskup, D. A. Jaroszynski, S. P. D. Mangles, A. G. R. Thomas, K. Krushelnick, and Z. Najmudin, "Evidence of photon acceleration by laser wake fields," Physics of Plasmas 13, 033108 (2006).
- ⁶⁰M. R. Edwards, K. Qu, Q. Jia, J. M. Mikhailova, and N. J. Fisch, "Cascaded chirped photon acceleration for efficient frequency conversion," Physics of Plasmas 25 (2018).
- ⁶¹Z. Nie, C. H. Pai, J. Hua, C. Zhang, Y. Wu, Y. Wan, F. Li, J. Zhang, Z. Cheng, Q. Su, S. Liu, Y. Ma, X. Ning, Y. He, W. Lu, H. H. Chu, J. Wang, W. B. Mori, and C. Joshi, "Rela-

- tivistic single-cycle tunable infrared pulses generated from a tailored plasma density structure," Nature Photonics **12**, 489–494 (2018).
- ⁶²E. Esarey, A. Ting, and P. Sprangle, "Frequency shifts induced in laser pulses by plasma waves," Physical Review A 42, 3526–3531 (1990).
- ⁶³V. A. Mironov, A. M. Sergeev, E. V. Vanin, G. Brodin, and J. Lundberg, "Upper limits for frequency up-conversion in the nonlinear photon accelerator," Physical Review A 46, R6178– R6180 (1992).
- ⁶⁴S. V. Bulanov, V. I. Kirsanov, F. Pegoraro, and A. S. Sakharov, "Charged particle and photon acceleration by wake field plasma waves in nonuniform plasmas," Laser Physics 3, 1078–1087 (1993).
- ⁶⁵A. J. Howard, D. Turnbull, A. S. Davies, P. Franke, D. H. Froula, and J. P. Palastro, "Photon Acceleration in a Flying Focus," Physical Review Letters 123, 124801 (2019).
- ⁶⁶ J. P. Palastro, J. L. Shaw, P. Franke, D. Ramsey, T. T. Simpson, and D. H. Froula, "Dephasingless laser wakefield acceleration," Phys. Rev. Lett. **124**, 134802 (2020).
- ⁶⁷A. Debus, R. Pausch, A. Huebl, K. Steiniger, R. Widera, T. E. Cowan, U. Schramm, and M. Bussmann, "Circumventing the Dephasing and Depletion Limits of Laser-Wakefield Acceleration," Physical Review X 9 (2019).
- ⁶⁸C. Caizergues, S. Smartsev, V. Malka, and C. Thaury, "Phase-locked laser-wakefield electron acceleration," Nature Photonics 14, 475–479 (2020).
- ⁶⁹S. V. Bulanov, V. A. Vshivkov, G. I. Dudnikova, N. M. Naumova, F. Pegoraro, and I. V. Pogorelsky, "Laser acceleration of charged particles in inhomogeneous plasmas i," *Plasma Physics Reports*, 23, 259–269 (1997).
- ⁷⁰P. Sprangle, B. Hafizi, J. R. Peñano, R. F. Hubbard, A. Ting, C. I. Moore, D. F. Gordon, A. Zigler, D. Kaganovich, and T. M. Antonsen, "Wakefield generation and GeV acceleration in tapered plasma channels," Physical Review E 63, 056405 (2001).
- ⁷¹E. Guillaume, A. Döpp, C. Thaury, K. Ta Phuoc, A. Lifschitz, G. Grittani, J.-P. Goddet, A. Tafzi, S. Chou, L. Veisz, and V. Malka, "Electron Rephasing in a Laser-Wakefield Accelerator," Physical Review Letters 115, 155002 (2015).
- ⁷²S. V. Bulanov, T. Z. Esirkepov, Y. Hayashi, H. Kiriyama, J. K. Koga, H. Kotaki, M. Mori, and M. Kando, "On some theoretical problems of laser wake-field accelerators," Journal of Plasma Physics 82, 905820308 (2016).
- ⁷³D. Guénot, D. Gustas, A. Vernier, B. Beaurepaire, F. Böhle, M. Bocoum, M. Lozano, A. Jullien, R. Lopez-Martens, A. Lifschitz, and J. Faure, "Relativistic electron beams driven by kHz single-cycle light pulses," Nature Photonics 11, 293–296 (2017).
- ⁷⁴ J. Kim, V. L. J. Phung, K. Roh, M. Kim, K. Kang, and H. Suk, "Development of a density-tapered capillary gas cell for laser wakefield acceleration," Review of Scientific Instruments 92, 023511 (2021).
- ⁷⁵R. T. Sandberg and A. G. R. Thomas, "Photon acceleration from optical to xuv," Phys. Rev. Lett. **130** (2023), 10.1103/Phys-RevLett.130.085001.
- ⁷⁶J. B. Rosenzweig, "Nonlinear plasma dynamics in the plasma wake-field accelerator," Physical Review Letters **58**, 555–558 (1987).
- ⁷⁷R. T. Sandberg and A. G. R. Thomas, "Dephasingless plasma wakefield photon acceleration," In preparation.
- ⁷⁸R. G. Hemker, Particle-in-Cell Modeling of Plasma-Based Accelerators in Two and Three Dimensions, Ph.D. thesis, UCLA (1999).
- ⁷⁹R. A. Fonseca, L. O. Silva, F. S. Tsung, V. K. Decyk, W. Lu, C. Ren, W. B. Mori, S. Deng, S. Lee, T. Katsouleas, and J. C. Adam, "Osiris: A three-dimensional, fully relativistic particle in cell code for modeling plasma based accelerators," in *Computational Science ICCS 2002*, edited by P. M. A. Sloot, A. G. Hoekstra, C. J. K. Tan, and J. J. Dongarra (Springer Berlin Heidelberg, Berlin, Heidelberg, 2002) pp. 342–351.
- ⁸⁰R. Lehe, M. Kirchen, I. A. Andriyash, B. B. Godfrey, and J. L.

- Vay, "A spectral, quasi-cylindrical and dispersion-free Particle-In-Cell algorithm," Computer Physics Communications **203**, 66–82 (2016).
- ⁸¹V. Yakimenko, L. Alsberg, E. Bong, G. Bouchard, C. Clarke, C. Emma, S. Green, C. Hast, M. Hogan, J. Seabury, N. Lipkowitz, B. O'Shea, D. Storey, G. White, and G. Yocky, "FACET-II facility for advanced accelerator experimental tests," Physical Review Accelerators and Beams 22, 101301 (2019).
- 82W. Mori, "The physics of the nonlinear optics of plasmas at relativistic intensities for short-pulse lasers," IEEE Journal of Quantum Electronics 33, 1942–1953 (1997).
- ⁸³ F. Li, T. N. Dalichaouch, J. R. Pierce, X. Xu, F. S. Tsung, W. Lu, C. Joshi, and W. B. Mori, "Ultra-bright electron bunch injec-

- tion in a plasma wakefield driven by a superluminal flying focus electron beam," (2021), arXiv:2108.00030 [physics.plasm-ph].
- ⁸⁴L. Oliveira e Silva and J. T. Mendonça, "Kinetic theory of photon acceleration: Time-dependent spectral evolution of ultrashort laser pulses," Phys. Rev. E **57**, 3423–3431 (1998).
- ⁸⁵T. Katsouleas, S. Wilks, P. Chen, J. M. Dawson, and J. J. Su, "Beam loading in plasma accelerators," Particle Accelerators 22, 81–99 (1987).
- ⁸⁶M. Tzoufras, W. Lu, F. S. Tsung, C. Huang, W. B. Mori, T. Katsouleas, J. Vieira, R. A. Fonseca, and L. O. Silva, "Beam loading by electrons in nonlinear plasma wakes," Physics of Plasmas 16, 056705 (2009).